Materials Research Proceedings **32** (2023) 330-337 https://doi.org/10.21741/9781644902615-38

Hot plastic behavior of an ultrafine-grained aluminum alloy fabricated by laser powder bed fusion and equal channel angular pressing

Jairo Alberto Muñoz[1,a*], Louis Huvelle[2,b], Enrique Manuel Huerta[1,c], and José María Cabrera[1,3,d]

[1]Department of Materials Science and Engineering EEBE, Universidad Politécnica de Catalunya, c/Eduard Maristany 10-14, 08019 Barcelona, Spain

[2]Ecole Européenne d'Ingénieurs en Génie des Matériaux EEIGM, Université de Lorraine, 6 Rue Bastien-Lepage, 54010 Nancy, France

[3]Fundació CIM-UPC, c/Llorens i Artigas 12, 08028 – Barcelona, Spain

[a]jairo.alberto.munoz@upc.edu, [b]louis.huvelle1@etu.univ-lorraine.fr, [c]enrique.manuel.huerta@upc.edu, [d]jose.maria.cabrera@upc.edu

Keywords: Additive Manufacturing (AM), Severe Plastic Deformation (SPD); Al Alloy, Plasticity

Abstract. This research presents the microstructural evolution and mechanical properties of a hypoeutectic AlSi11Cu alloy obtained through laser powder bed fusion (L-PBF) and subsequent severe plastic deformation. The as-built alloy demonstrated a structure formed by an Al matrix surrounded by a Si-enriched cellular network. Tensile tests indicated a yield strength of 350 MPa and elongation to fracture lower than 5% for the as-built material. After subjecting the alloy to severe plastic deformation (SPD) using equal channel angular pressing (ECAP), superior mechanical properties such as an elongation almost twice as high as the as-built condition (12% compared to 6%) and a high tensile yield strength (320 MPa) were observed. ECAP produced average grain size reduction from 10 μm in the as-built state to 1 μm after six ECAP passes. Microstructural analyses highlight in particular the grain refinement of the microstructure after the ECAP process, changing from a microstructure composed of columnar grains to a heterogeneous microstructure characterized by ultra-fine (grain sizes between 200 nm - 500 nm) and elongated grains (grains between 5 μm – 10 μm). This finding supposes a huge improvement for the mechanical performance of this alloy breaking the strength-ductility paradox. The superplastic properties of the materials were characterized, depending on the variation of the temperature and strain rate parameters. This showed that the superplastic behavior was favored by low strain rates (here 0.001 s^{-1}), and by increasing temperature (400 °C). Thus, elongations exceeding 70% were achieved with ECAP material.

Introduction

Throughout human history, great efforts have been made to develop structural materials with optimized mechanical properties for applications in different areas of industry, such as civil, medical, transportation, aerospace, and energy. Also, several manufacturing processes have been stablished amount them additive manufacturing (AM) and severe plastic deformation (SPD). AM also known as 3D printing processes have been attracting attention in recent years, because it could easily be adapted to generate alternative processing routes. AM is an industry that has existed for more than 30 years and has rapidly gained public and commercial interest due to its advantages in printing complex geometries without using assembly processes [1]. The development of these technologies is driven by a reduction in manufacturing cycle times, improved durability but also a reduction in manufacturing costs. These development paths have enabled additive manufacturing to find its way into many sectors such as aeronautics, aerospace, automotive and biomedicine [2].

According to ISO/ASTM 52900 [3], additive manufacturing is characterized as a process of assembling materials to make parts from 3D model data. Currently, the American Society for Testing and Materials (ASTM International) groups additive manufacturing into seven different families: Binder jetting, Directed energy deposition (DED), Material extrusion, Material jetting, Laser Powder Bed Fusion (L-PBF), sheet lamination, and vat photopolymerization. L-PBF is considered today as one of the most promising 3D printing techniques. This process, which takes place in a controlled atmosphere (e.g., argon) at high heating and cooling rates (e.g., 10^3 until 10^8 K s^{-1}), uses a high-energy laser beam to completely melt the metal powder [4]. This technique allows the production of very high-quality parts with excellent mechanical properties due to the heterogenous and complex microstructures [5]. However, the thermal gradients and the repetitive fusion of powder layers give rise to high residual stresses, lack of fusion, and porosity that affect funtional properties like mechanical strength and ductility [6,7].

On the other hand, metallic materials produced by severe plastic deformation (SPD) techniques possessing ultrafine grain structures have been shown to have unique mechanical, chemical and physical properties that can lead them to meet the demands of different industries. SPD processes are defined as metal forming processes in which a large deformation is introduced into a metal in order to produce metals with ultrafine grain sizes. The advantage of this type of grain refinement techniques is the attractive mechanical properties of the produced parts, such as high strength and a remarkable lightness, which are generally superior than their coarse-grained counterparts. As well as providing a significant improvement in material properties, SPD is a relatively simple process and there have been many ways in which the process has been improved to suit specific shapes and large parts [8,9]. Although ultrafine-grained (UFG) materials can exhibit a 2-3-fold increase in strength over material in the annealed state, it is also true that UFG materials exhibit mechanical inconvenience due to lack of strain hardening. This lack of hardening promotes limited homogeneous ductility. For this reason, the search for a high ductility combined with a high strength have been the objective of many investigations carried out during the last years [10,11]. In this context, there are several properties (e.g., microstructure and tensile behavior at high homologous temperatures), types of materials and new manufacturing routes such as the combination of AM and SPD that have not yet been studied and explored in great detail. Therefore, these topics represent a new field of study in search of materials with outstanding properties that require attention from the research community.

This research work brings together several well-known technologies: additive manufacturing, using the Laser Powder Bed Fusion (LPBF) method, which is a technology with great potential for large-scale use in industry, severe plastic deformation (SPD), using the Equal Channel Angular Pressing (ECAP) process, allowing materials to have novel microstructural and mechanical properties. Therefore, microstructural characterization using Electron Back Scattering Diffraction (EBSD) and tensile tests at room and hot temperatures for the as-built, and ECAP processed conditions were analyzed.

Materials and methods

The studied material is an almost eutectic aluminum-silicon alloy AlSi11Cu manufactured by L-PBF with the chemical composition indicated in Table 1. The metallic powders used to print the material were produced at the Volgograd Aluminium Plant (UC RUSAL), in Russia, using the molten metal spraying method. 20 mm diameter and 100 mm length rods were manufactured at the National University of Science and Technology (MISIS) in Moscow (Russia) using a selective laser melting (SLM) SLM280HL printer with the following operating conditions: scan speed of V = 1650 mm/s, layer thickness H = 50 μm, power of W = 370 W, and hatch spacing of 130 μm. Different samples for mechanical tests and microstructure characterization were cut-out of the rods using electrode discharge machining (EDM).

Materials Research Proceedings **32** (2023) 330-337 https://doi.org/10.21741/9781644902615-38

Table 1 Chemical composition of the studied alloy.

Element	Si	Cu	Mn	Mg	Ti	Zn	Fe	Pb	Ni	Ca	Al
Wt. %	10.6	0.78	0.54	0.47	0.25	0.21	0.03	0.03	0.01	0.01	Bal.

For the ECAP process an hydraulic press of 80 Tons was used. The ECAP die was designed with an inner angle of 120°, and the material was processed at 250 °C for six ECAP passes. This temperature was used because at room temperature the ECAP process produced cracks in the samples. Route B_C and Molybdenum disulfide (MoS_2) as lubricant were used to process the samples.

To characterize the alloy microstructure, a scanning electron microscope (SEM) Jeol, model JSM-7001F coupled with an EBSD detector operating at 15 eV and probe current of 14 A was used. Sample surfaces were prepared by mechanical polishing using carbon silicon sand papers and diamonds suspensions of 9 µm, 6 µm, 3 µm, and 1 µm. A final polishing step with colloidal silica of 0.03 µm particle size on a vibratory machine for 3 h was carried out to get a smooth surface free of scratches. Data was acquired with HKL Channel 5 software and analyzed with TSL-OIM 7.3b. Grains with less than 2 pixels were excluded from any statistical analysis. Optical microscopy (OM) and Kellers reagent were used to revel the melting pools before and after ECAP processing.

The mechanical properties of the specimens at room temperature were tested by means of uni-axial tensile tests using the Deben Microtest Tensile Stage machine. To measure the strain during the tensile tests, a so-called digital image correlation (DIC) non-contact technique was used. DIC analysis were carried out using a video correlation system equipped with one camera Balser of 5 MP and resolution of 2448 x 2048 at 75 fps. For a good illumination, one LED lightning grids was used. The deformation data was acquired using the Software VIC Gauge 2D for video extensometer purposes. The hot tensile tests were carried out using the Instron 5407 machine, coupled with a water-cooled infrared (IR) heater. Different temperatures and strain rates were analyzed.

Results and discussion

Fig. 1 gives the feedstock and as-built (AB) material characteristics using OM and SEM. Fig. 1a shows the powders spherical particles using SEM. With this image, some characteristics of the powders are obtained, such as the size of the particles and their size distribution, represented on Fig. 1b. Particles show an average size of 24.5 µm with a standard deviation of 8,8 µm. Some granulometric values are also calculated such as $d10$ = 13.6 µm, $d50$ = 23.6 µm, and $d90$ = 36.8 µm. This particle size distribution according to several researches is appropriate for a good powder flowability during the LPBF process [12]. Thus, powders can spread evenly on the powders bed, according to EPMA (European Powder Metallurgy Association (EPMA) and EuroAM (European Additive Manufacturing Group) [13]. Fig. 1c shows several layers of melting pools (MP) for the as-built material, which is the result of the selective fusion of powders during the L-PBF process. At high magnifications, SEM allows observing microstructural characteristics inside both the MP and the melting pool boundaries (MPB), as indicated in Fig. 1d and Fig. 1e. At this magnification, the structure of the alloy reveals an eutectic light-colored interconnected network (Si-rich zone) and a dark-colored cellular matrix (Al matrix). Inside the MPB, the interconnected network is expanded, elongated, unlike inside the MP, where the interconnected network is less expanded, showing a more equiaxed structure, as corroborated by Fig. 1f and Fig. 1g, respectively. This difference in structure may be due to melting/solidification/re-melting cycles between the printing layers, so some areas are subject to temperature gradients that reach higher values during printing. As MPBs are the boundary of two melting zones, they are more affected by this phenomenon.

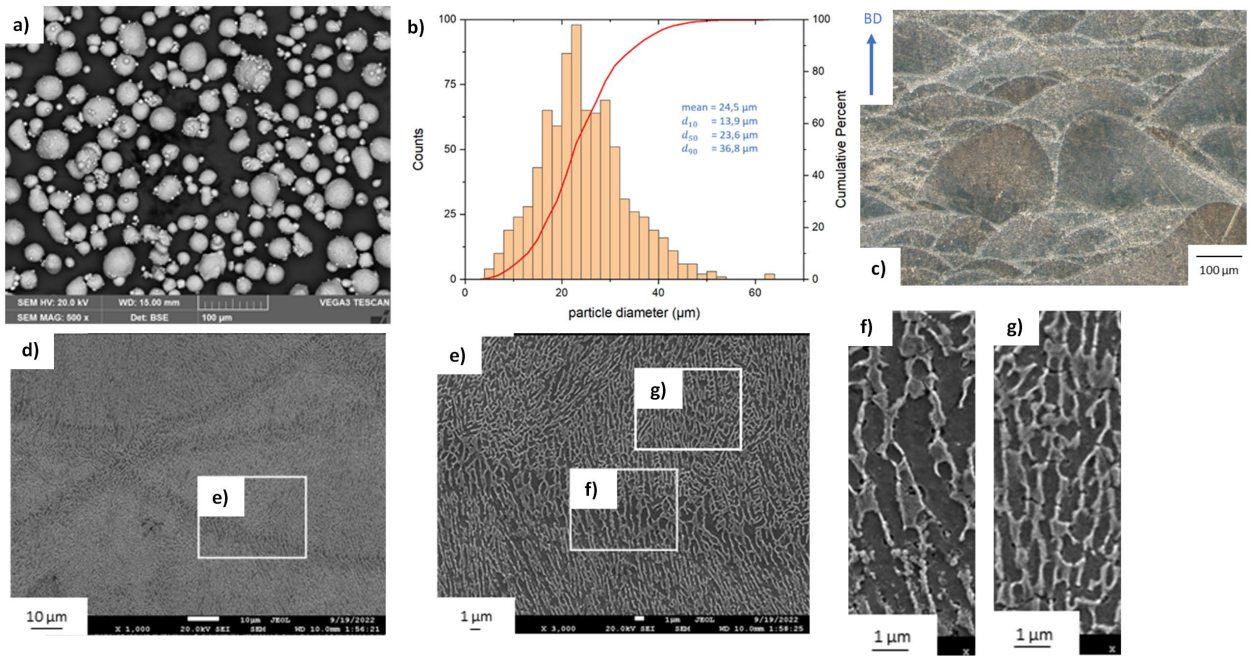

Fig. 1 a) SEM image of the initial powders, b) powders distribution size, c) as-built material, d) SEM image for the as-built material, e) SEM image close to one melting pool boundary, f) SEM image inside the melting pool boundary, and g) SEM image inside the melting pool.

Fig. 2a and Fig. 2b show the optical microstructure after SPD by 6 ECAP passes. Some differences on the optical microstructure are observed with respect to the AB condition. The ECAP process produced a shear effect on the optical microstructure, which is now characterized by elongated and rotated MPs. In this figure, significant microstructural changes can be observed. MPs are still visible and their height have been significantly reduced. Fig. 2c highlights that ECAP processing has resulted in significant microstructural changes. For example, the Si-rich network is destroyed after ECAP processing and the Al cellular structure is not as evident as in the AB condition, giving rise to a microstructure with a high density of particles.

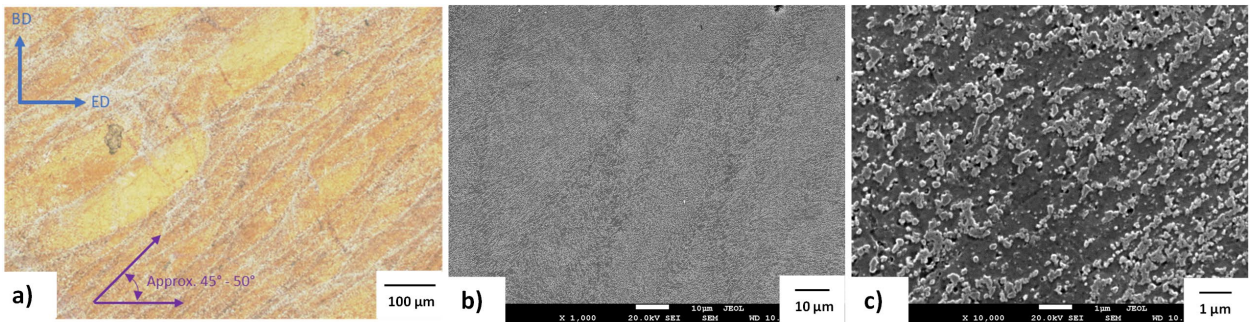

Fig. 2 a) Optical micrography for the ECAP processed material, b) SEM image after six ECAP passes, and c) cellular structure breakdown after six ECAP passes.

The microstructural characterization of the AB and ECAP materials can be followed by EBSD analyses, as shown in Fig. 3a and Fig. 3b, respectively. The low and high angle grain boundaries (LABG and HAGB) are also highlighted in white and black colors, respectively. The inverse pole figure (IPF) map of the AB material shows that the MPs present a morphology composed by columnar grains, while small and equiaxed grains are located around the MPBs. Thus, the grain

Materials Research Proceedings **32** (2023) 330-337 https://doi.org/10.21741/9781644902615-38

size distribution for the AB material is represented by a single symmetric peak curve, suggesting an average grain size of ~10 µm. For the six ECAP passes material, different types of grains are visible on the IPF map of Fig. 3b. The grain size distribution on Fig. 3b suggests an average grain size of ~1 µm, which is 10 times smaller than the AB material. Although, there are still grains that have not been well refined, as the distribution shows the existence of some large grains that measure 20 µm approximatively. This behavior is coherent with the not-symmetric grain size distribution for the ECAP material concerning the like-Gauss function distributions observed on the AB condition, which corroborates a heterogeneous microstructure that mix ultrafine grains (UFGs) with coarse grains (CGs).

Fig. 4a and Fig. 4b show the tensile true and engineering stress-strain curves for all the studied conditions. The AB materials has a yield tensile strength (YTS) of 393 MPa, an ultimate tensile strength (UTS) of 565 MPa, a uniform elongation (Eu) and elongation at fracture (Ef) of 4.6% and 4.9%, respectively. It should be noted that the AB material has better mechanical properties than similar alloys produced by traditional forming processes (such as casting). Indeed, according to D. Song et al. such a cast alloy presents a YTS of 115 MPa, a UTS of 140 MPa, and elongation of 2,2% [14]. On the other hand, the ECAP processed material reached a YTS and UTS of 319 MPa and 494 MPa, respectively. The lower mechanical properties for the ECAP processed than the AB material can be related to the interconnected network breakdown, as shown in Fig. 2c. This behavior is related with the smooth strain hardening rate curve displayed on Fig. 4b for the ECAP processed material, while the AB condition presents a curve with multiple peaks leading to the strain localization according to the Considère criteria in Eq. (1) [15]. Thus, the interconnected network breakdown allows space for the dislocation motion and the new particles also generate a pinning effect maintaining a larger tensile ductility than the AB material.

$$\frac{d\sigma}{d\varepsilon} \geq 0. \tag{1}$$

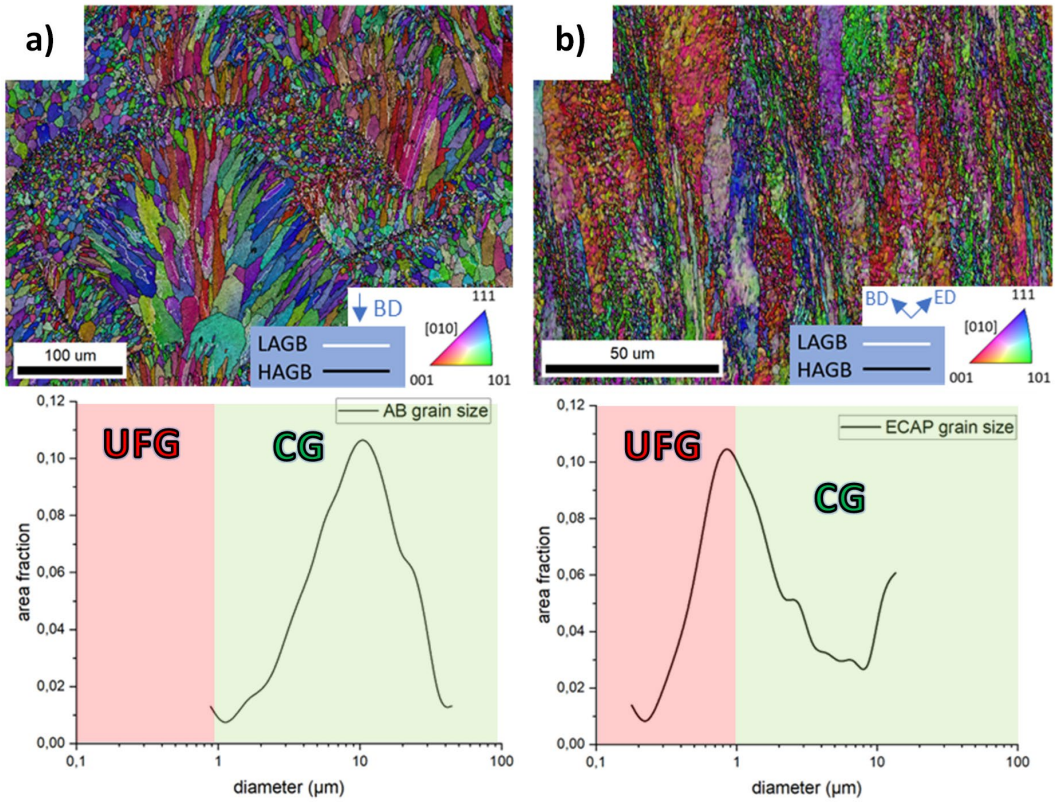

Fig. 3 EBSD analysis for the a) as-built and b) ECAP processed materials.

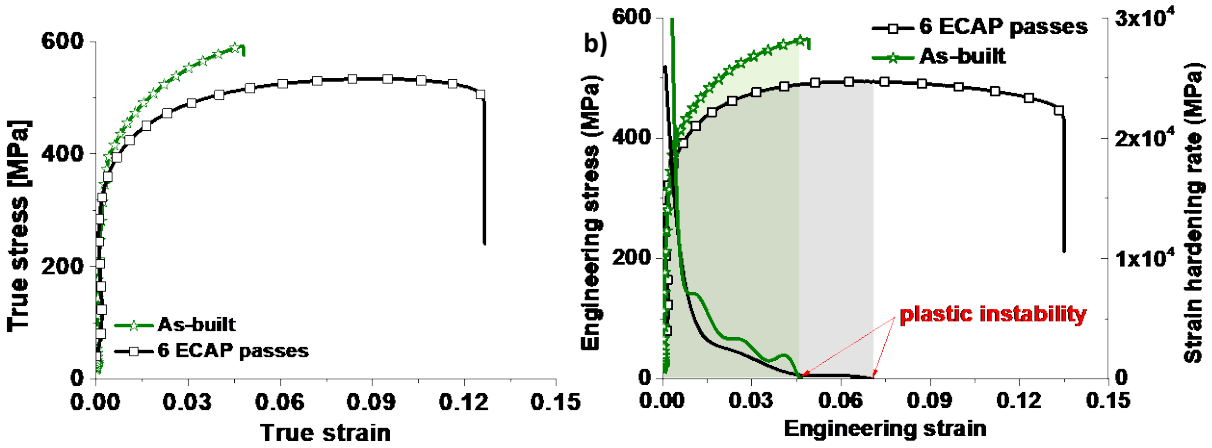

Fig. 4 a) True stress-strain curves and b) engineering stress-strain and strain hardening rate curves for the analyzed materials.

Fig. 5 indicates the hot tensile curves and some microstructures for different temperatures and strain rates. As the temperature increases the maximum stress decreases and elongation increases. This is well correlated with the grain size growth as the temperatures used correspond to homologues temperatures of $0.52T_M$, $0.61T_M$, and $0.69T_M$ the alloys melting temperature (T_M). Therefore, recovery and recrystallization phenomena occurred, as observed on the EBSD maps and tensile curves. At temperatures between 300 °C and 350 °C the EBSD maps on Fig. 5a and Fig. 5b show equiaxed grains with heterogeneous grain sizes, while at 400 °C a clear grain growth together with grains smaller than 1 µm are observed on Fig. 5c. Thus, the ECAP processed condition reached elongations around 70%, but did not show any superplastic behavior after 6 ECAP passes. This could be attributed to the heterogeneous microstructure, which was not fully UFG like the research work of Jiang Jing-hua et al. [16] on an as-cast AlSi11 alloy processed by sixteen ECAP passes with an average grain size of 300 nm. However, it can be stablished that the ECAP processing after the LPBF process is a good processing route to improve the strength-ductility of AM materials.

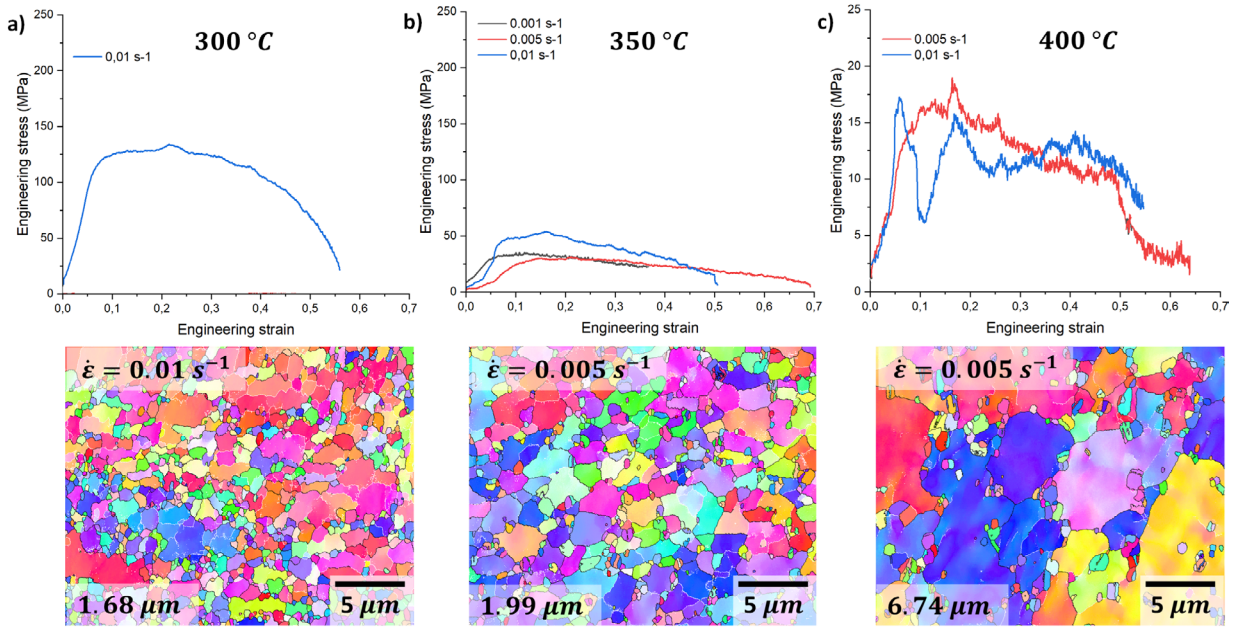

Fig. 5 Hot tensile curves and microstructures for the six ECAP passes material a different temperatures and strain rates, a) 300 °C, b) 350 °C, and c) 400 °C.

Summary

The ECAP processing of an AlSi11Cu alloy manufactured by L-PBF produced a heterogeneous microstructure with an excellent combination of strength-ductility. The ECAP process transformed the interconnected network into particles and reduced the melting pools heigh due to the compression and shear strain components during the extrusion process. These changes conducted to a better tensile plasticity because of the increased space for the dislocation motion and the pinning effect with the new particles. In terms of superplastic behavior, the ECAP processed alloy did not reach elongations beyond 70%, but the grain size showed a good thermal stability until 350 °C.

References

[1] W.J. Sames, F.A. List, S. Pannala, R.R. Dehoff, S.S. Babu, The metallurgy and processing science of metal additive manufacturing, Int. Mater. Rev. 61 (2016) 315–360. https://doi.org/10.1080/09506608.2015.1116649

[2] M. Pérez, D. Carou, E.M. Rubio, R. Teti, Current advances in additive manufacturing, Procedia CIRP. 88 (2020) 439–444. https://doi.org/https://doi.org/10.1016/j.procir.2020.05.076

[3] I. Astm, ASTM52900-15 standard terminology for additive manufacturing—general principles—terminology, 2015.

[4] J. Gunasekaran, P. Sevvel, I. John Solomon, Metallic materials fabrication by selective laser melting: A review, Mater. Today Proc. 37 (2021) 252–256. https://doi.org/https://doi.org/10.1016/j.matpr.2020.05.162

[5] J.A. Muñoz, S. Elizalde, A. Komissarov, J.M. Cabrera, Effect of heat treatments on the mechanical and microstructural behavior of a hypoeutectic Al alloy obtained by laser powder bed fusion, Mater. Sci. Eng. A. 857 (2022) 144091. https://doi.org/https://doi.org/10.1016/j.msea.2022.144091

[6] W. Chen, T. Voisin, Y. Zhang, J.-B. Florien, C.M. Spadaccini, D.L. McDowell, T. Zhu, Y.M. Wang, Microscale residual stresses in additively manufactured stainless steel, Nat. Commun. 10 (2019) 4338. https://doi.org/10.1038/s41467-019-12265-8.

[7] Y. Li, K. Zhou, P. Tan, S.B. Tor, C.K. Chua, K.F. Leong, Modeling temperature and residual stress fields in selective laser melting, Int. J. Mech. Sci. 136 (2018) 24–35. https://doi.org/https://doi.org/10.1016/j.ijmecsci.2017.12.001

[8] A. Azushima, R. Kopp, A. Korhonen, D.Y. Yang, F. Micari, G.D. Lahoti, P. Groche, J. Yanagimoto, N. Tsuji, A. Rosochowski, A. Yanagida, Severe plastic deformation (SPD) processes for metals, CIRP Ann. 57 (2008) 716–735. https://doi.org/https://doi.org/10.1016/j.cirp.2008.09.005

[9] K. Edalati, A. Bachmaier, V.A. Beloshenko, Y. Beygelzimer, V.D. Blank, W.J. Botta, K. Bryła, J. Čížek, S. Divinski, N.A. Enikeev, Y. Estrin, G. Faraji, R.B. Figueiredo, M. Fuji, T. Furuta, T. Grosdidier, J. Gubicza, A. Hohenwarter, Z. Horita, J. Huot, Y. Ikoma, M. Janeček, M. Kawasaki, P. Král, S. Kuramoto, T.G. Langdon, D.R. Leiva, V.I. Levitas, A. Mazilkin, M. Mito, H. Miyamoto, T. Nishizaki, R. Pippan, V. V Popov, E.N. Popova, G. Purcek, O. Renk, Á. Révész, X. Sauvage, V. Sklenicka, W. Skrotzki, B.B. Straumal, S. Suwas, L.S. Toth, N. Tsuji, R.Z. Valiev, G. Wilde, M.J. Zehetbauer, X. Zhu, Nanomaterials by severe plastic deformation: review of historical developments and recent advances, Mater. Res. Lett. 10 (2022) 163–256. https://doi.org/10.1080/21663831.2022.2029779

[10] X. Wu, Y. Zhu, Heterogeneous materials: a new class of materials with unprecedented mechanical properties, Mater. Res. Lett. 5 (2017) 527–532. https://doi.org/10.1080/21663831.2017.1343208

[11] Y. Zhu, X. Wu, Heterostructured materials, Prog. Mater. Sci. 131 (2023) 101019. https://doi.org/https://doi.org/10.1016/j.pmatsci.2022.101019

[12] Additive Manufacturing Overview, in: Addit. Manuf. Process., ASM International, 2020. https://doi.org/10.31399/asm.hb.v24.9781627082907

[13] Metal Powders key features, (2020). https://www.epma.com/additive-manufacturing (accessed April 29, 2023).

[14] D. Song, G. Wang, Z. Zhou, E.E. Klu, B. Gao, A. Ma, Y. Wu, J. Sun, J. Jiang, X. Ma, Developing a high-strength Al–11Si alloy with improved ductility by combining ECAP and cryorolling, Mater. Sci. Eng. A. 773 (2020) 138880. https://doi.org/10.1016/j.msea.2019.138880

[15] A. Considère, Memoire sur l'emploi du fer et de l'acier dans les constructions, Ann. Des Ponts Chaussées l Sem. 9 (1885) 574–775.

[16] J. Jiang, A. Ma, N. Saito, A. Watazu, P. Lin, Y. Nishida, Effect of microstructures on superplasticity of Al-11%Si alloy, Trans. Nonferrous Met. Soc. China. 17 (2007) 509–513. https://doi.org/https://doi.org/10.1016/S1003-6326(07)60124-1